electronics

Article

A Stationary Reference Frame Current Control Algorithm for Improvement of Transient Dynamics of a Single Phase Grid Connected Inverter

Horyeong Jeong and Jae Suk Lee *

Department of Electrical Engineering, Jeonbuk National University, Jeonju 54896, Korea; bumbu13@naver.com
* Correspondence: jaesuk@jbnu.ac.kr

Received: 4 March 2020; Accepted: 23 April 2020; Published: 27 April 2020

Abstract: This paper proposes a stationary reference frame current control algorithm for a single-phase grid-connected inverter (GCI) for improvement of transient dynamic performance. Disturbance, i.e., grid voltage in a target system, is estimated using a stator current observer, and the estimated disturbance is applied to a current controller for implementation of disturbance rejection control (DRC). In the proposed current control algorithm, the disturbance rejection control algorithm is applied to reduce the overcurrent occurring in the single-phase grid-connected inverter when grid faults happen. In this paper, the AC phase current of a single-phase inverter is controlled, instead of the current vector, which is a DC signal. To compensate for the drawbacks of controlling the AC phase current, such as phase lag and steady-state error, command feedforward control is also applied in the proposed control system. The proposed control algorithm is mathematically derived and represented in transfer functions and implemented via simulation and experiment.

Keywords: grid connected inverter; command feedforward control; disturbance rejection control

1. Introduction

Nowadays, the greenhouse effect is a significant issue in the world, and the largest amount of greenhouse gas is carbon dioxide, which is produced by use of fossil energy. Use of renewable energy is one approach to reduce the greenhouse effect, and electricity generation using wind power and solar energy has been increased. For the generation and utilization of electric energy, AC to DC rectification and DC to AC inverting processes are essential, and the development of topologies and control algorithms for electric power converters have received attention [1,2]. When electric power is generated through a three-phase power system, one of the three-phase power lines is connected to a residential grid system. Therefore, a single-phase grid-connected inverter (GCI) is used for residential applications, for example, a photovoltaics (PV) power generation system and a vehicle to grid (V2G) system [3,4]. When a grid fault such as a line-to-ground fault occurs, transient current may reach its limit depending on fault conditions and the transient current can result in a trip or damage components in a GCI system. Accidents due to overcurrent can be prevented through hardware (a fuse or a circuit breaker) or software (control algorithms) approaches. Control algorithms for a GCI system can be categorized depending on the reference frame, such as a stationary or synchronous reference frame. Since DC signals are controlled in a synchronous reference frame current control system, phase lag or steady-state error with respect to frequency can be negligible. However, phase angle information is required for reference frame transformation, and a phase locked loop (PLL) should be implemented in a synchronous reference frame current control system. PLL algorithms have been developed to improve their performance [5,6] because they determine the performance of a system. However, PLL algorithms become complicated when trying to improve their performance, and an additional AC signal is needed to implement PLL for a single-phase application [7,8]. Unlike a three-phase system, a virtual AC signal should be developed for reference frame transformation for a single-phase system. Besides the added complexity, development of a virtual AC signal is an additional process for the single-phase system, and unexpected deviation may occur during the development of a virtual AC signal or due to the developed virtual AC signal during reference frame transformation. A proportional-resonance (PR) controller is one of the GCI current controllers implemented in a stationary reference frame [9,10]. Using PR control, bandwidth at a specific resonance frequency can be designed to be infinite ideally, and designated harmonic components can be eliminated selectively. Therefore, PR control is used for the purpose of power quality improvement in a grid system application. If the number of harmonics orders to be eliminated is increased, the number of PR controllers needs to be increased. A stationary reference frame proportional-integral (PI) current controller has been presented for a GCI current control system [11,12]. Though a stationary reference frame PI current control system does not require reference frame transformation and can avoid a PLL and cross-coupling between the d and q axes, phase lag or steady-state error with respect to frequency causes degradation of system performance. To compensate for the drawbacks, command feedforward (CFF) controllers were developed using low pass filter parameters and applied to a GCI control system in [13–16]. Using the CFF controllers, reduction of steady-state error and total harmonic distortion (THD) in current is achieved. In [17], model predictive control (MPC) was applied in a GCI current control system. Future dynamics can be estimated using MPC, and the estimated future dynamics are used to achieve optimization objectives such as zero steady-state error of grid current. Therefore, command tracking performance at a stationary reference frame GCI current control system can be improved through control algorithms using CFF and MPC. Along with command tracking performance at steady state, the transient dynamics and robustness of a control system with respect to disturbance are also important performance metrics. In a GCI current control system, grid voltage is regarded as a disturbance. When a grid fault occurs, transient grid current may trip a GCI system or damage components in the system. To solve this issue, disturbance observer based control (DOBC) and active disturbance rejection control (ADRC) algorithms have been presented [18–21]. Using DOBC and ADRC, disturbance to the systems is estimated, and stability and robustness improvement of target applications is achieved using the estimated disturbance in the control system.

In this paper, command feedforward control and disturbance rejection control (DRC) algorithms are developed and applied to a stationary reference frame PI current controller of a single-phase GCI system with an LCL filter. The proposed control algorithm is developed to improve robustness of a system to disturbance (grid fault) and to protect a GCI system by improving transient dynamics and reducing peak current at the moment of a grid accident. In the following sections, the proposed current control algorithm is derived and analyzed in time and frequency domains. The proposed algorithm is implemented and verified in simulations and experiments.

2. Command Feedforward Control for a GCI Current Control System

Figure 1 shows a graphical representation of a single-phase GCI system with residential distributed generation (DG) applications such as PV solar power generation and a V2G system. The overall system consists of a single-phase GCI located between DG applications and the single-phase AC grid system, a grid current control system including gate drivers, voltage modulation and a PI current controller for operating the insulated–gate bipolar transistor (IGBT) switches. It also contains an LCL filter to reduce harmonics generated during the switching process.

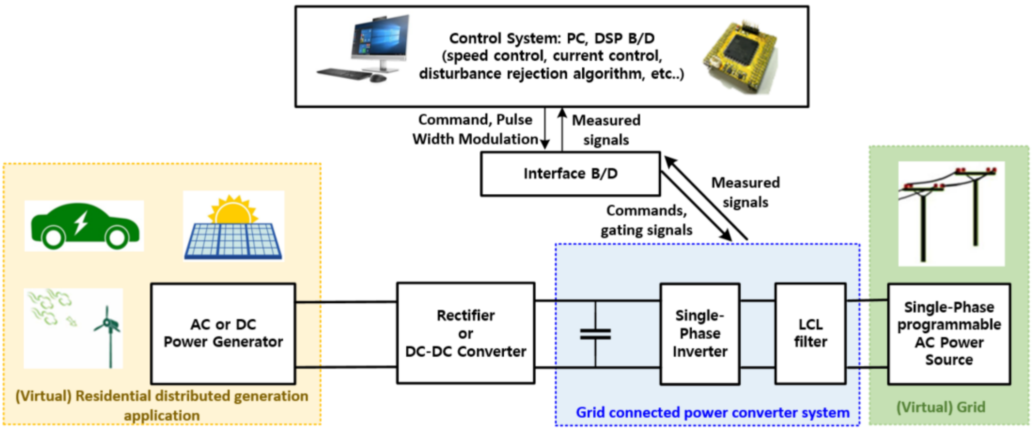

Figure 1. A graphical representation of residential distributed generation with a single-phase GCI control system.

In the proposed control algorithm, phase (AC) current is controlled instead of current vector, which is a DC signal. By controlling the AC signal, steady-state error and phase delay may occur. To compensate for the drawbacks, command feedforward control is applied to the proposed algorithm. A system block diagram of a single-phase GCI current control system with command feedforward control is shown in Figure 2.

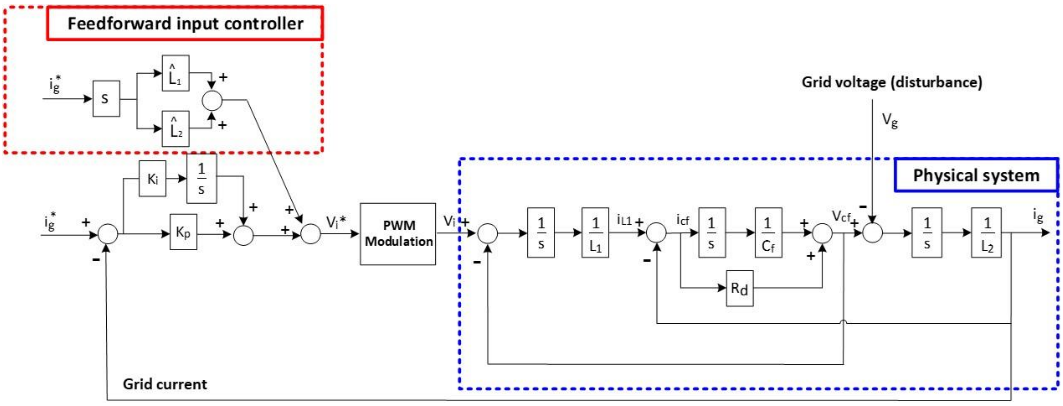

Figure 2. A system block diagram with command feedforward control.

In Figure 2, a PI controller is used for single-phase grid current control and the physical system of the given control system is an LCL filter. The transfer function of the physical system is derived as (1), and V_i and i_g are inverter output voltage and grid current respectively.

$$\frac{i_g}{V_i} = \frac{1 + R_d\, C_f s}{L_1 L_2 C_f s^3 + R_d C_f (L_1 + L_2) s^2 + (L_1 + L_2) s} \tag{1}$$

Parameters and variables used in Figure 2 and a transfer function (1) are defined in Table 1 below. In this paper, * and ˆ denote command signal and estimated value respectively.

Table 1. Definition of variables in a GCI current control system.

L_1	Inverter side LCL filter inductance	i_g	Grid current
L_2	Grid side LCL filter inductance	V_g	Grid voltage
C_f	LCL filter capacitance	K_P	Proportional controller gain
R_d	Damping resistance	K_i	Integral controller gain

The command feedforward controller is designed using an inverse model of the physical system, an LCL filter in the system. In this paper, the inverse model is simplified by neglecting R_d and C_f to avoid complexity of the command feedforward controller structure. Using the transfer function of the LCL filter and the simplified inverse model, transfer functions of a single phase GCI current control system with and without command feedforward control are derived as Equations (2) and (3) respectively.

$$\frac{i_g}{i_g^*} = \frac{R_d C_f K_p s^2 + (K_p + R_d C_f K_i)s + K_i}{L_1 L_2 C_f s^4 + R_d C_f (L_1 + L_2) s^3 + (L_1 + L_2 + R_d C_f K_p) s^2 + (K_p + R_d C_f K_i)s + K_i} \quad (2)$$

$$\frac{i_g}{i_g^*} = \frac{R_d C_f \left(\hat{L_1} + \hat{L_2}\right) s^3 + (\hat{L_1} + \hat{L_2} + R_d C_f K_p) s^2 + \left(K_p + R_d C_f K_i\right) s + K_i}{L_1 L_2 C_f s^4 + R_d C_f (L_1 + L_2) s^3 + (L_1 + L_2 + R_d + C_f K_p) s^2 + (K_p + R_d C_f K_i)s + K_i} \quad (3)$$

Using Equations (2) and (3), bode plots of the stationary reference frame and proposed current control systems are drawn and shown in Figure 3.

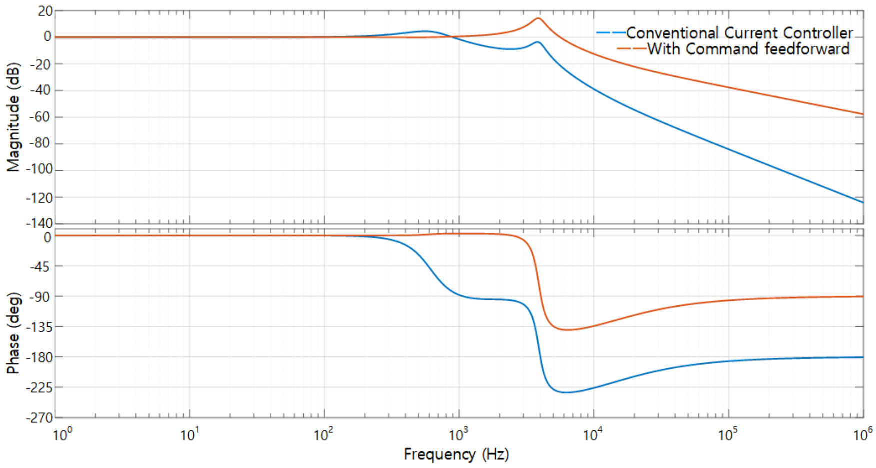

Figure 3. Bode plots of the conventional and proposed GCI current control systems.

As shown in Equations (2) and (3), compensation of the steady-state error and the phase delay can be expected by applying command feedforward control. From Figure 3, it is shown that a bandwidth is wider with the same controller gain and phase lag is reduced using the proposed single-phase grid current control method. That is, command tracking performance of the control system can be improved compared to the case without the command feedforward controller.

3. Disturbance Rejection Control for Single-Phase GCI Current Control Systems

When grid voltage faults occur in a grid system, overcurrent occurs, which may damage the electrical circuits or components in a GCI. One of the methods to prevent overcurrent due to the grid voltage fault is applying disturbance rejection to the GCI system. The disturbance can be effectively rejected by feedforwarding opposite polarity voltage of the grid voltage measured by a voltage sensor. Since the disturbance is reflected to a controller in real time, disturbance can be eliminated in real time, and the load of a controller due to disturbance can be reduced. If a sensor or an interface board is damaged, the measured signal from a sensor can be distorted, and the distorted signal is used for controlling a system. Therefore, disturbance in the system is estimated through a single-phase grid current observer and used for disturbance rejection in the proposed control algorithm as a back-up for measured signal from a voltage sensor. Figure 4 shows the proposed single-phase GCI current control system with a single-phase grid current observer.

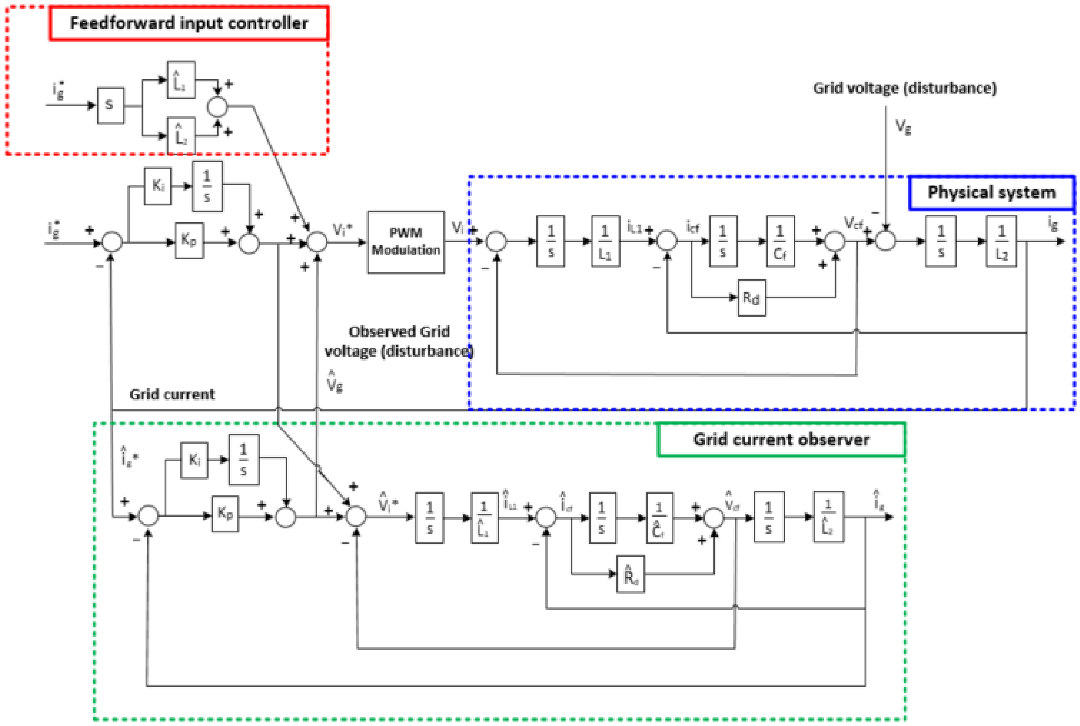

Figure 4. A system block diagram with a single-phase grid current observer for disturbance rejection in a single-phase GCI current control system.

As shown in Figure 4, the single-phase grid current observer is developed using physical system parameters and the PI current controller output of the GCI current control system in Figure 4. If the single-phase grid current observer is properly developed, an intermediate signal of the current observer gives the estimated grid voltage ($\hat{V}g$) and can be summed as a feedforward signal to the output of the PI controller. Thus, the actual grid voltage in the physical system can be estimated using the single-phase grid current observer. Then, the estimated grid voltage can be applied to the single-phase current PI controller instead of the measured voltage from a voltage sensor. The estimated grid voltage can be used to reject disturbance of the GCI system, and disturbance to the GCI system can be effectively eliminated.

Dynamic stiffness is defined as disturbance required for the unit change of the output signal and is one of the metrics representing robustness of the system to disturbance. From Figure 4, transfer functions representing dynamic stiffness are derived in Equations (4) and (5) assuming estimated disturbance is identical to actual disturbance.

$$\frac{v_g}{i_g} = \frac{L_1L_2C_fs^4+R_dC_f(L_1+L_2)s^3+(L_1+L_2+R_d+C_fK_p)s^2+(K_p+R_dC_fK_i)s+K_i}{L_1C_fs^3+R_dC_fs^2+s} \tag{4}$$

$$\frac{v_g}{i_g} = \frac{L_1L_2C_fs^4+R_dC_f(L_1+L_2)s^3+(L_1+L_2+R_d+C_fK_p)s^2+(K_p+R_dC_fK_i)s+K_i}{L_1C_fs^3} \tag{5}$$

Using Equations (4) and (5), dynamic stiffness plots of the conventional and proposed control systems are shown in Figure 5.

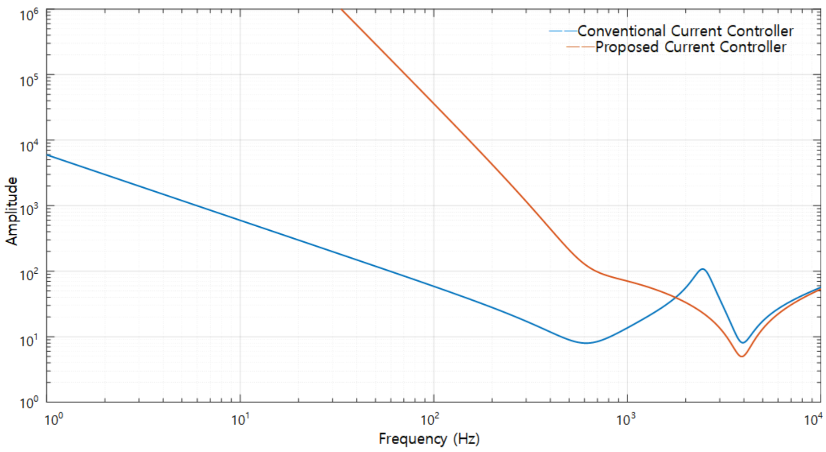

Figure 5. Dynamic stiffness of the conventional and proposed GCI current control system.

As shown in Figure 5, resonance property at the resonant frequency area and dynamic stiffness at low frequency, including main operational frequency range (50–60 Hz), are improved using the proposed GCI current control method.

4. Simulation Results and Analysis

In this section, simulation results of single-phase GCI current control methods are shown. The proposed GCI current control method, the PR controller at the stationary reference frame and the PI current controller at the synchronous reference frame are implemented in simulation for performance comparison. The simulation was implemented using PLECS software. The sample time used for the simulation is 100 (μsec). It is assumed that the reference signal of a single-phase GCI current control system is generated using the method presented in [22] during simulation. Furthermore, command feedforward control and disturbance rejection control are applied to the conventional and the proposed methods for comparison of performance. The GCI system and controller parameters used for simulations and experiments in this paper are summarized in Table 2.

Table 2. GCI system and controller parameters.

Parameter	Value	Parameter	Value
Grid voltage (V_g)	110 [V_{AC}]	Inverter side inductor (L_1)	1.5 [mH]
Frequency	50 [Hz]	Filter capacitor (C_f)	2.75 [μF]
DC link voltage	350 [V_{DC}]	Damping resistor (R_d)	4.9 [Ω]
Switching frequency	10 [kHz]	Grid side inductor (L_2)	1 [mH]
Proportional gain (K_p)	10	Integral gain (K_i)	40,000

If a disturbance to the GCI current control system is ideally decoupled or rejected by the estimated disturbance applied to the current controller, reduction of the peak value of transient grid current is expected. Accuracy of grid voltage estimation determines the performance of the proposed single-phase GCI current control system. Figure 6 shows the simulation results of the disturbance estimated using the single-phase grid current observer.

Figure 6 shows a comparison of actual and estimated grid voltage and error between two signals. As shown in the simulation results, the estimation error of the disturbance is below 5%, besides for the transient region. In the simulation and experiment, the estimated grid voltage is feedforwarded to a single-phase current controller for disturbance rejection purposes instead of the measured grid voltage from the voltage sensor.

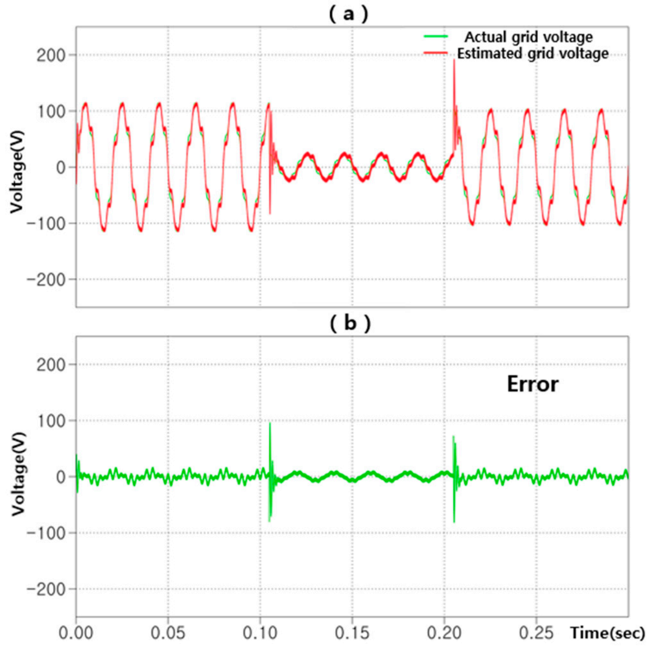

Figure 6. Simulation results of measured actual grid voltage and estimated grid voltage through the single-phase grid current observer, (**a**) actual and estimated grid voltage (**b**) error between actual and grid voltage.

Figure 7 shows a comparison of the phase current at the inverter side and the grid side when conventional and the proposed GCI current control algorithms are implemented in simulation.

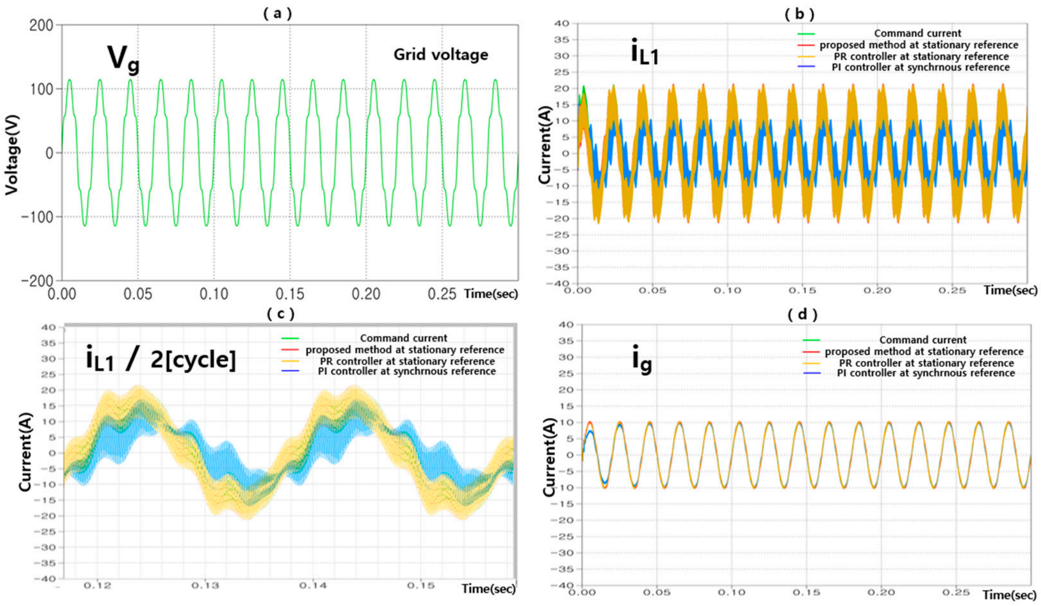

Figure 7. Simulation results of grid voltage and phase current responses of the GCI current control system. (**a**) grid voltage, (**b**) inverter side current (**c**) grid side current at a full time range and (**d**) zoomed in inverter side current.

As conventional current control methods, PR control and PI control at the synchronous reference frame are implemented in simulation, and disturbance rejection is applied to all current control methods. During simulation, distorted grid voltage by 5th and 7th harmonics shown in Figure 7 (i) is applied as disturbance to a GCI current control system. As shown in Figure 7 (ii) and (iii), the command tracking performance (steady-state error and phase lag) of each control method is almost identical. In addition, THD is another steady-state performance to be analyzed because the power quality should satisfy international standards for grid connection. THD and root mean square (rms) values of the phase current at an inverter side and grid side are summarized in Table 3.

Table 3. Summary of steady-state simulation results in Figure 7.

Control Method	Reference Frame	THD	Inverter Side Current (i_{L1})	Grid Side Current (i_g)
PI controller (Proposed)	Stationary	4.4 [%]	11.98 [A_{rms}]	7.07 [A_{rms}]
PR controller	Stationary	5 [%]	11.93 [A_{rms}]	7.08 [A_{rms}]
PI controller	Synchronous	4.2 [%]	8.05 [A_{rms}]	7.07 [A_{rms}]

As shown in the Table 3, the THD results of each current controller are below 5%, which satisfies the grid code. The THD and rms values of the inverter side phase current using a PI current controller at the synchronous reference frame show the minimum value compared to other phase current controllers. It is because the DC signals are controlled in a synchronous reference frame that the THD and rms values of the inverter side phase current are minimum. THD using the PR controller can be reduced more if PR controllers eliminating harmonic components are added.

Not only steady-state operation but also grid voltage fault condition is implemented in simulation. As a grid fault situation in the single-phase grid system, a single-phase line-to-ground fault is implemented, and simulation results of the current control for a single-phase GCI are shown in Figure 8.

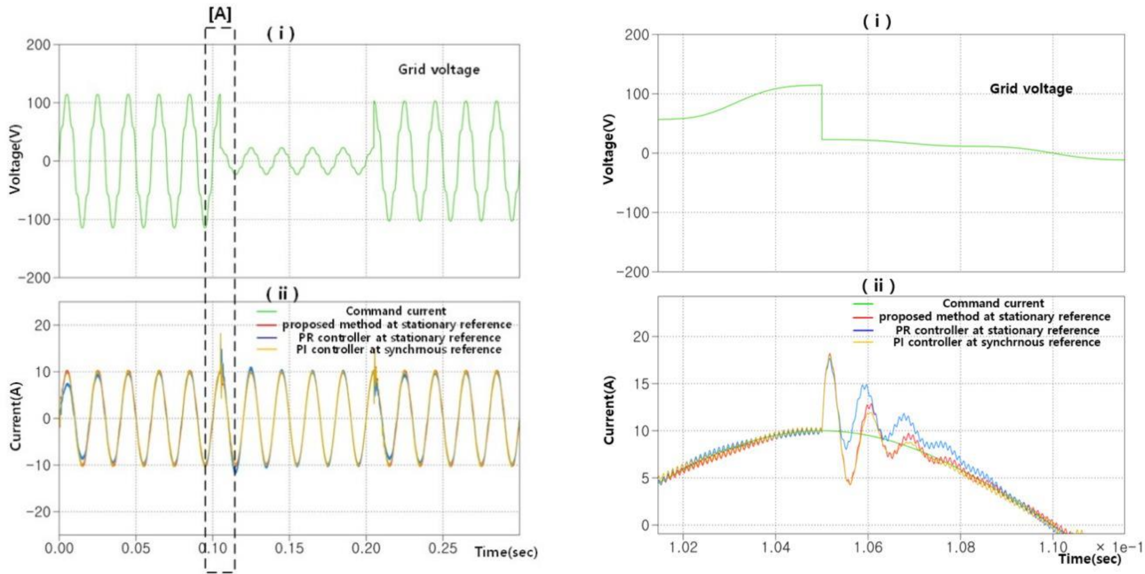

(**a**) (**b**)

Figure 8. Simulation results of (**i**) grid voltage and (**ii**) grid current when line-to-ground grid voltage fault occurs. (**a**) simulation results at a full time range (**b**) zoomed in simulation results of (**a**).

Figure 8 shows simulation results of grid voltage and grid current when the conventional and the proposed phase current control methods are applied. The simulation results in Figure 8b are zoomed in results on [A] region in Figure 8a. When grid fault occurs, grid voltage magnitude is reduced to 20% of its nominal value in the simulation. As shown in Figure 8, the phase current of a single-phase GCI system is controlled properly using the conventional and proposed methods at steady state. When grid fault happens at the moment of [A] in Figure 8a, transient grid current is observed. The simulation results in Figure 8 are summarized in Table 4 below. The reduction ratio of the peak current is calculated using Equation (6).

$$\text{Reductionratio} = \frac{\text{PeakcurrentwithoutDRC} - \text{PeakcurrentwithDRC}}{\text{PeakcurrentwithoutDRC}} \quad (6)$$

Table 4. Summary of simulation results at grid fault in Figure 8.

Control Method	Reference Frame	Peak Current [A_{peak}]		Reduction Ratio
		without DRC	with DRC	
PI controller (Proposed)	Stationary	20.15	18.21	9.6%
PR controller	Stationary	19.43	17.71	8.8%
PI controller	Synchronous	19.96	18.09	9.3%

As shown in the simulation results in Figure 8 and Table 4, the peak current is reduced for all single-phase grid current controllers by applying the disturbance rejection controller proposed in this paper. Though DC signals are controlled in a synchronous reference frame PI current controller, it is investigated that the peak value of the phase current is almost identical to the peak current that occurred using the stationary reference frame current controllers. This is because the distorted phase angle during the grid fault is used for the reference transformation in a synchronous reference frame PI current control system. From the simulation results, it is verified that the peak phase current value can be reduced when a grid fault occurs, and almost the same level of performance is obtained when compared to the other two approaches but with lower complexity using the proposed current control method.

5. Experimental Results

This section shows the experimental results of the conventional and proposed control algorithm. The parameter values used in the experiment and operating conditions are identical to the parameter values in the simulation shown in Table 2. During the experiment, the grid fault condition and various orders of harmonics voltage generation were emulated using the three-phase programmable AC power supply shown in Figure 9a. A control board using a Texas Instrument F28377S MCU DSP chip is responsible for overall system control and signal processing. Mitsubishi Intelligent Power Modules (IPMs) are used for an inverter and a rectifier of the system. The rectifier is used for substituting a battery pack in an electric vehicle or DC power generation from a PV system. In addition, a heatsink is used to reduce the heat generated from IPMs during operation. The experimental setup is shown in Figure 9.

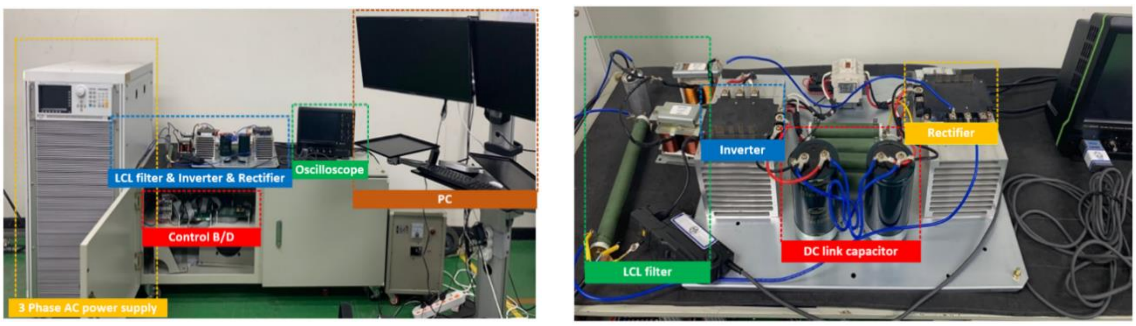

(**a**) (**b**)

Figure 9. (**a**) Experimental set-up, (**b**) a GCI and a passive low pass filter.

Figure 10a,b show measured voltage and phase current when the proposed single phase GCI current control method is applied. As shown in the experimental results, phase current is properly controlled without steady state error and phase lag using the proposed single-phase GCI current control method. The high frequency noise on the grid current signal seems to be coming from a sensor interface board or connection between a scope and a current probe.

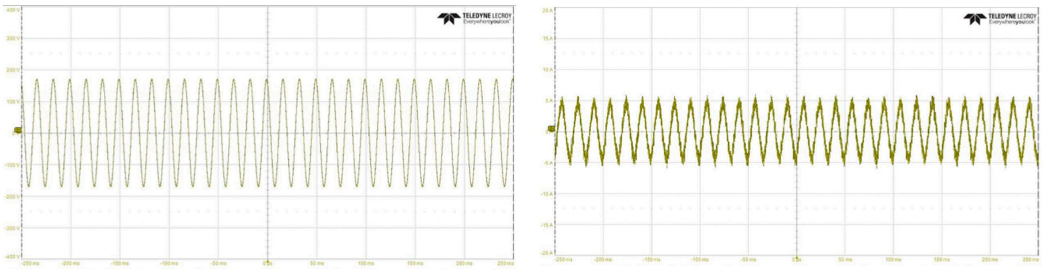

(**a**) (**b**)

Figure 10. Experimental results of (**a**) grid voltage and (**b**) phase current when the proposed single-phase current control method is applied.

Figure 11 shows the experimental results when a grid fault occurs. Figure 11a is the estimated grid voltage using the single-phase grid current observer when the single-phase grid voltage fault occurs. Since the experimental results of the estimated grid voltage in Figure 11a are data recorded through a digital signal processor, it is not able to be superimposed with the measured grid voltage during the experiment. Figure 11b shows the grid current when a voltage fault occurs. From the experimental results in Figure 11, it is verified that the grid current can be controlled properly when a grid fault occurs in the grid system using the proposed current control method.

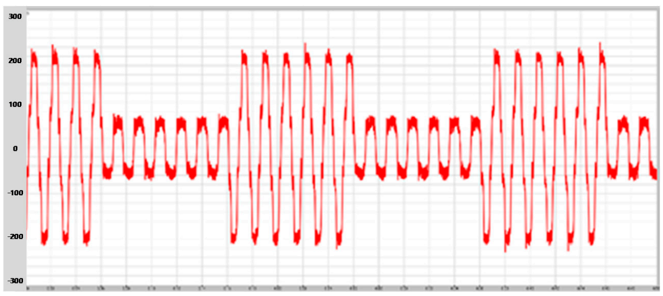

(**a**) Estimated grid voltage using the single-phase grid current observer

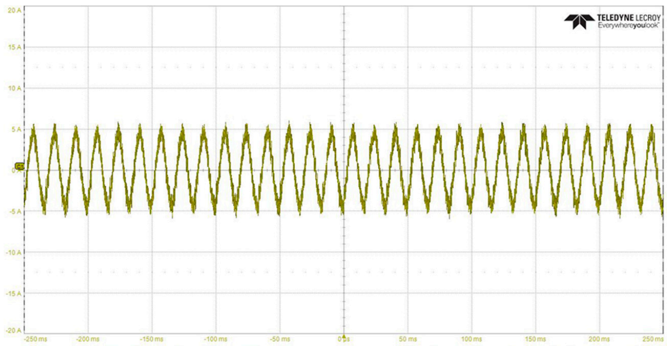

(**b**) Measured grid current

Figure 11. Experimental results when the proposed current control method is used under line-to-ground grid voltage fault condition.

6. Conclusions

This paper presents a stationary reference frame single-phase current control algorithm for a GCI system to reduce peak value of grid current when a grid fault occurs and to improve command tracking performance. For implementation of the proposed algorithm, the command feedforward control and the disturbance rejection control using the single-phase grid current observer are applied to a stationary reference frame PI current control. Command tracking performance and robustness to disturbance of the proposed single-phase GCI current control algorithm are analyzed in the frequency domain through a bode plot and dynamic stiffness. As well as in the frequency domain, the characteristics of the proposed method are analyzed and compared with conventional control methods in the time domain. Using the proposed single-phase GCI current control algorithm, peak current is reduced when a grid voltage fault occurs. Not only command tracking performance is improved using the proposed current control algorithm by reducing steady-state error and phase lag but also power quality improvement is shown by comparing the THD of the phase current. The proposed control algorithm for a single-phase GCI system is implemented in a simulation and experiment, and it is verified that almost the same level of performance can be obtained compared to the other two approaches but with lower complexity using the proposed current control method.

Author Contributions: H.J. implemented simulations and experiment for this paper and J.S.L. proposed the control algorithms and advised writing this paper. All authors have read and agreed to the published version of the manuscript.

Funding: This research is funded by Korea Electric Power Corporation through Korea Electrical Engineering & Science Research Institute [grant number: R17XA05-7]. This research was supported by "Research Base Construction Fund Support Program" funded by Jeonbuk National University in 2020.

Acknowledgments: This research is supported by Korea Electric Power Corporation through Korea Electrical Engineering & Science Research Institute [grant number: R17XA05-7]. This research was supported by "Research Base Construction Fund Support Program" funded by Jeonbuk National University in 2020.

Conflicts of Interest: The authors declare no conflicts of interest.

References

1. Albatran, S.; Smadi, I.; Ahmad, H.; Koran, A. Online optimal switching frequency selection for grid connected voltage source inverters. *Electronics* **2017**, *6*, 110.
2. Baek, J.; Choi, W.; Chae, S. Distributed control strategy for autonomous operation of hybrid AC/DC microgrid. *Energies* **2017**, *10*, 373.
3. Ngo, T.; Lee, K.; Won, J.; Nam, K. Study of single-phase bidirectional battery charger for high power application. In Proceedings of the 7th International Power Electronics and Motion Control Conference, Harbin, China, 2–5 June 2012; pp. 958–962.
4. Jain, S.; Agarwal, V. A single stage grid connected inverter topology for solar PV systems with maximum power point tracking. *IEEE Trans. Power Electr.* **2007**, *22*, 1928–1940.
5. Guan, Q.; Zhang, Y.; Kang, Y.; Guerrero, J. Single phase phase locked loop based on derivative elements. *IEEE Trans. Power Electr.* **2016**, *32*, 4411–4420.
6. Lai, N.; Kim, K. An Improved Current Control Strategy for a Grid-Connected Inverter under Distorted Grid Conditions. *Energies* **2016**, *9*, 190.
7. Zhang, Q.; Sun, X.; Zhong, Y.; Matsui, M.; Ren, B. Analysis and design of a digital phase locked loop for single phase grid connected power conversion systems. *IEEE Trans. Ind. Appl.* **2011**, *58*, 3581–3592.
8. Brabandere, K.; Loix, T.; Engelen, K.; Bolsen, B.; van den Keybus, J.; Driesen, J.; Belman, R. Design and operation of a phase locked loop with Kalman Estimator-based filter for single-phase applications. In Proceedings of the IECON 2006—32nd Annual Conference on IEEE Industrial Electronics, Paris, France, 6–10 November 2006.
9. Teodorescu, R.; Blaabjerg, F.; Liserre, M.; Loh, P. Proportional resonant controllers and filters for grid connected voltage source converters. *IET Proc. Electr. Power Appl.* **2006**, *153*, 750–762.
10. Shen, G.; Zhu, X.; Zhang, J.; Xu, D. A new feedback method for PR current control of LCL filter based grid connected inverter. *IEEE Trans. Ind. Appl.* **2010**, *57*, 2033–2041.

11. Rodriguez, P.; Luna, A.; Munoz-Aguilar, R.; Etxeberria-Otadui, I.; Teodorescu, R.; Blaabjerg, F. A stationary reference frame grid synchronization system for thee phase grid connected power converters under adverse grid conditions. *IEEE Trans. Power Electr.* **2012**, *27*, 99–112.
12. Vasquez, J.; Guerrero, J.; Savaghebi, M.; Garcia, J.E.; Teodorescu, R. Modeling, Analysis, and Design of Stationary-Reference-Frame Droop-Controlled Parallel Three-Phase Voltage Source Inverters. *IEEE Trans. Ind. Electr.* **2013**, *60*, 1271–1280.
13. Ryan, M.J.; Brumsickle, W.E.; Lorenz, R.D. Control topology options for single phase UPS inverters. *IEEE Trans. Ind. Appl.* **1997**, *33*, 493–501.
14. Abdel-Rahim, N.M.; Quaicoe, J.E. Analysis and design of a multiple feedback loop control strategy for single phase voltage source UPS inverter. *IEEE Trans. Power Electr.* **1996**, *11*, 532–541.
15. Ma, L.; Luna, A.; Rocabert, J.; Munos, R.; Corcoles, F.; Rodriguez, P. Voltage feed-forward performance in stationary reference frame controllers for wind power applications. In Proceedings of the 2011 International Conference on Power Engineering, Energy and Electrical Drives, Malaga, Spain, 11–13 May 2011.
16. Zmood, N.; Holmes, D. Stationary frame current regulation of PWM inverters with zero steady state error. *IEEE Trans. Power Electr.* **2003**, *18*, 814–822.
17. Ahmed, K.; Massoud, A.; Finney, S.; Williams, B. A modified stationary reference frame based predictive current control with zero steady state error for LCL coupled inverter based distributed generation systems. *IEEE Trans. Ind. Electr.* **2011**, *58*, 1359–1370.
18. Chen, W.H.; Ballance, D.J.; Gawthrop, P.J.; Member, S.; Reilly, J.O.; Member, S. A Nonlinear Disturbance Observer for Robotic Manipulators. *IEEE Trans. Ind. Electr.* **2000**, *47*, 932–938.
19. Sariyildiz, E.; Ohnishi, K. Stability and robustness of disturbance observer-based motion control systems. *IEEE Trans. Ind. Electr.* **2015**, *62*, 414–422.
20. Pizzocaro, M.; Calonico, D.; Calosso, C.; Clivati, C.; Costanzo, G.A.; Levi, F.; Mura, A. Active disturbance rejection control of temperature for ultra-stable optical cavities. *IEEE Trans. Ultrason. Ferroelectr. Freq. Control* **2013**, *60*, 273–280. [PubMed]
21. Yang, J.; Cui, H.; Li, S.; Zolotas, A. Optimized Active Disturbance Rejection Control for DC-DC Buck Converters with Uncertainties Using a Reduced-Order GPI Observer. *IEEE Trans. Circuits Syst. I Regul. Papers* **2018**, *65*, 832–841.
22. Zhao, X.; Chang, L. Active and reactive power decoupling control of grid connected inverters in stationary reference frame. *Chin. J. Electr. Eng.* **2017**, *3*, 18–24.